Supporting Information

Sulfide SE	Ionic Conductivity ($S\ cm^{-1}$)	Electronic conductivity# ($S\ cm^{-1}$)	Ea (eV)	Stability (V)	Ref
Li_6PS_5Cl (LPSCl), Li_6PS_5X) *	$\sim 3.7 \times 10^{-3}$	$\sim(5.1 \times 10^{-6})$ [51] $\sim(10^{-8})$ [52,53]	~0.30- 0.40	1.71-2.01	[51,52,53,54]
β-Li_3PS_4 (LPS)*	$\sim 1.6 \times 10^{-4}$	$\sim(10^{-9}-10^{-8})$ [55] $\sim(10^{-5})$[53]	0.49 ± 0.02 [56] ~0.27-0.31[55]	1.71-2.31	[56,55]
$Li_7P_3S_{11}$ (LPS)	$\sim 17 \times 10^{-3}$	-	~0.17	2.28-2.31	[57]
Li_7GePS_8 (Aka tetragonal LGPS)	$\sim 10 \times 10^{-3}$	-	~0.22	-	[58]
$Li_{10}GeP_2S_{12}$ (LGPS)	$\sim 12 \times 10^{-3}$	$\sim 10^{-8}$	~0.21	1.7-2.15[59]	[58]
$Li_{10}SnP_2S_{12}$ (LSnPS)	$\sim 4 \times 10^{-3}$	$\sim(10^{-8}$ to $10^{-9})$[60]	~0.27 (Grain) ~0.60 (GB)	-	[60]
$Li_{11}Si_2PS_{12}$ (LSiPS)	$\sim 25 \times 10^{-3}$	-	~0.19	-	[61]

ESI-1. *Table: Key properties of the currently considered promising and highly explored sulphide-based solid ion conductors in the literature*

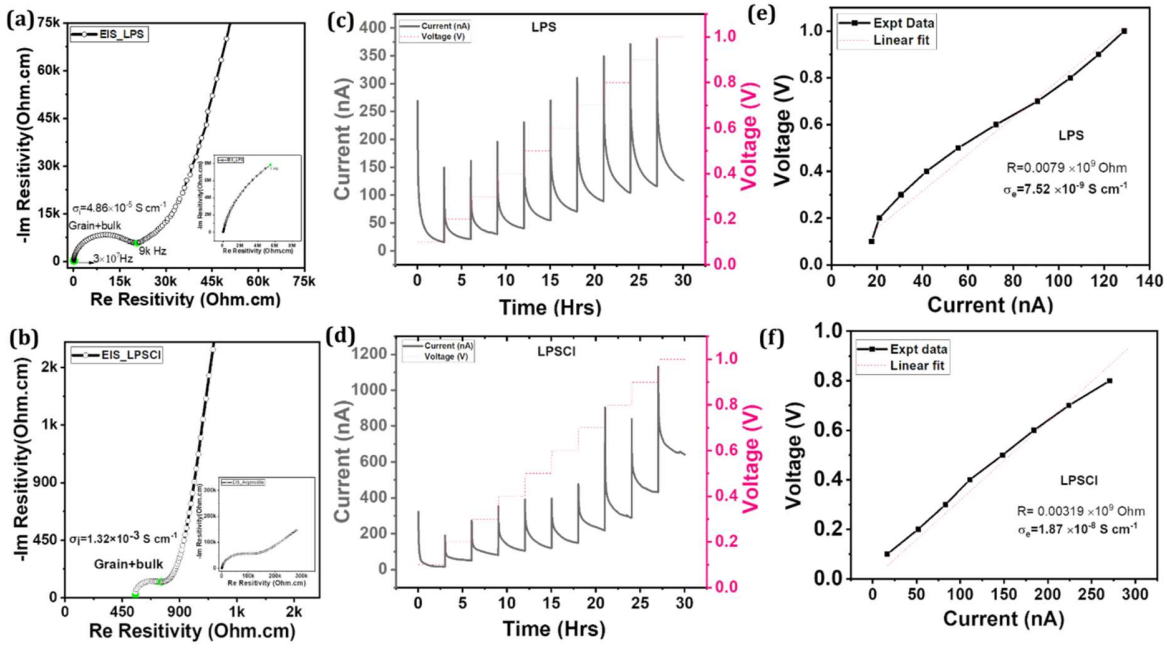

ESI-2. *Nyquist plot of (a) β- LPS (b) LPSCl, DC polarization experiment in (c) β- LPS (d) LPSCl and (e) and (f) show plot of Voltage vs Current for the resistance calculation obtained via Ohms law (V=IR) for LPS and LPSCl respectively.*

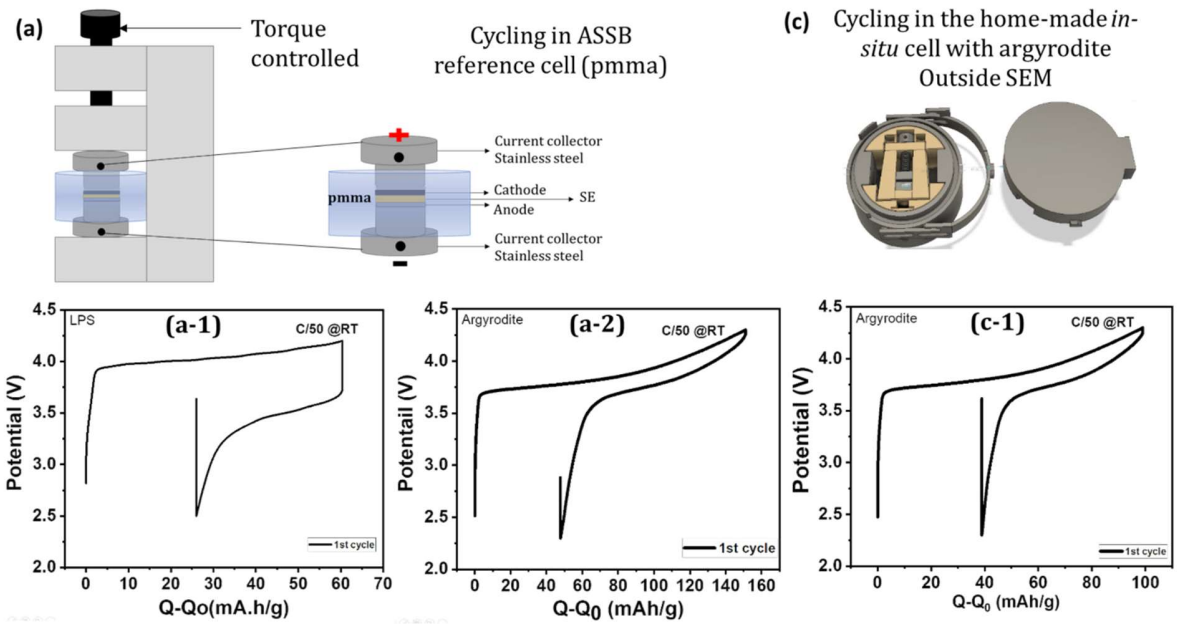

ESI-3. *(a) Reference cycling set-up for verification/comparison of the electrochemistry with the newly developed in-situ cell. The system consists of a pmma matrix with two stainless-steel pistons which are again placed under an axial screw which controls the torque applied. (a-1) shows the electrochemistry of LPS-SE with the reference system (a-2) shows the electrochemistry of LPSCl-SE with the reference system. (c) shows the in-situ cell cycling system and (c-1) shows the electrochemistry with LPSCl cycled outside SEM with a full 10 mm pellet with an in-situ cell. All the cycling data are at Room temperature. This confirms the reliability of the electrochemistry with the newly developed cell*

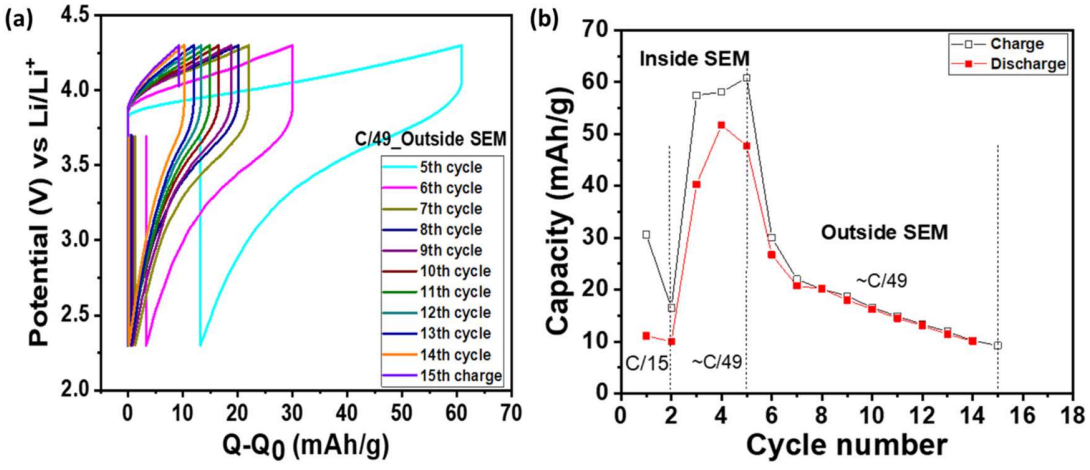

ESI-4. *(a) "In-situ cell" using argyrodite SE cycling outside SEM, from 5th discharge and showing a constant capacity fade with increasing cycles and (b) Capacity vs cycle number for the entire experiment (in-situ and ex-situ cycling.*

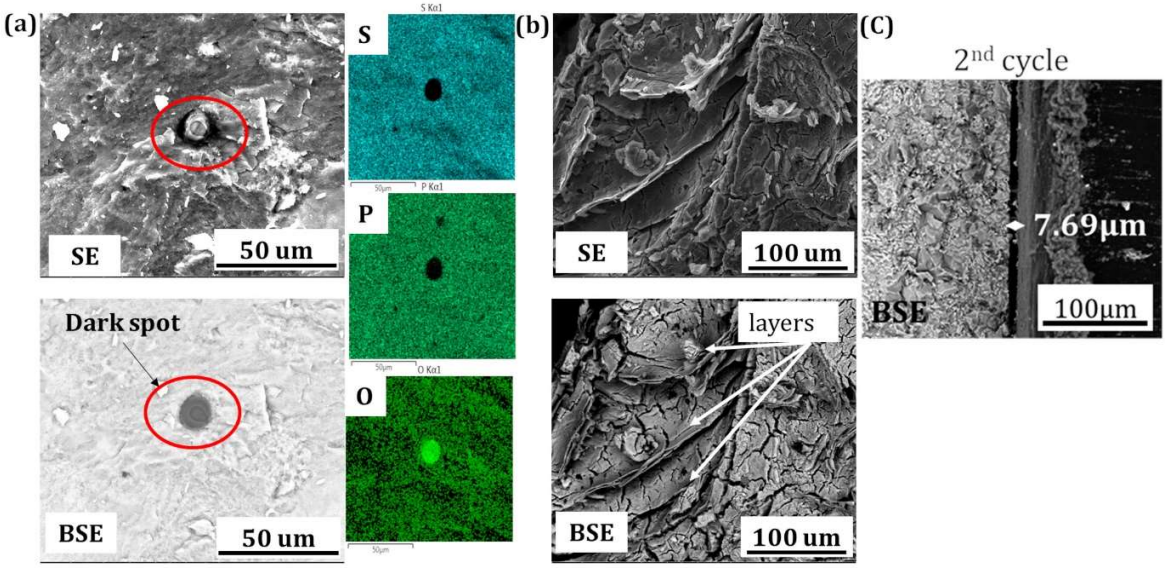

ESI-5. *(a) secondary (SE) and backscattered (BSE) electrons images of dark spots in LPS solid electrolyte together with EDS mapping on sulfur (S), phosphorus (P) and Oxygen (O). (b) secondary (SE) and backscattered (BSE) electrons images of LPS layered morphology at the cross-section. c) backscattered (BSE) electrons images of the loss of contact at lithium interface in LPSCl by the end of the 2nd cycle.*

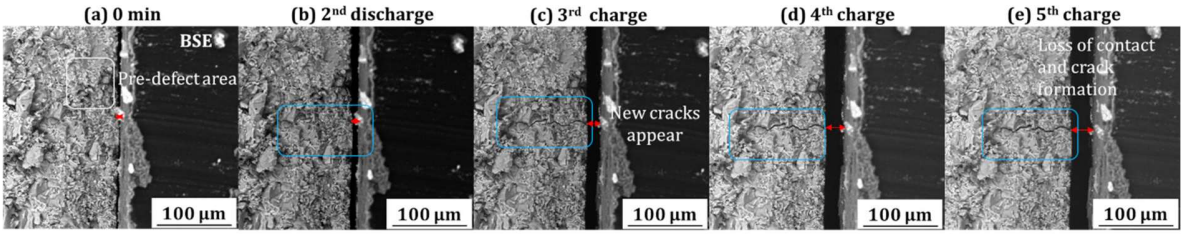

ESI-6: Growth of pre-defect, crack formation in LPSCl-SE at the (-) negative/anode interface.

White rectangles show the pre-defect area, Light blue rectangles show the new crack and growth of cracks in the LPSCl-SE from an existing pre-defect or an area nearby and the red arrow indicates the contact loss at the anode interface.

(a) 0 min shows the presence of a pre-defect area and the small red arrow at LPSCl/Li interface shows good contact. (b) An incision mark of crack and small, loss of contact begin to appear (c) by the end of 3rd charge, new cracks appear in the LPSCl shown with blue rectangles. (d) The contact loss grows further. (e) The cracks and contact loss grow even further by the end of the 5th charge.

All the images shown here are backscattered secondary electron images (BSE). Irrespective of the interface, crack formation and growth in LPSCl occurs either at the pre-defect or close by areas to the pre-defect.

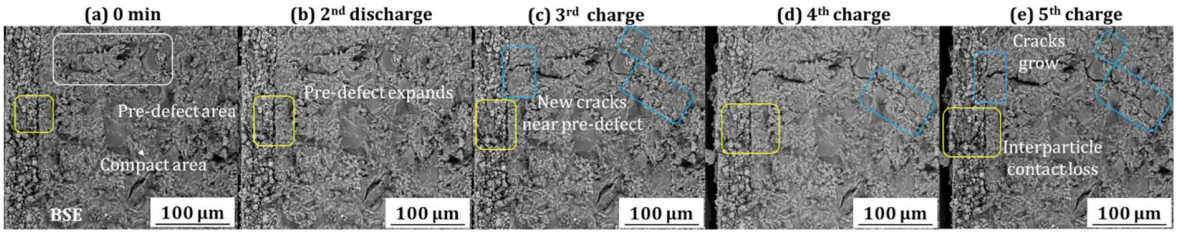

***ESI-7*: Growth of pre-defect, crack formation in LPSCl-SE at the (+) positive/cathode interface.**

White rectangles show the pre-defect area, Light blue rectangles show the new crack formation and growth from an existing pre-defect or an area nearby. The yellow rectangle shows the growth of the crack in the cathode composite of LPSCl.

(a) 0 min shows the presence of a pre-defect area, a compact area in the SE, and an area marked with a yellow rectangle in the cathode composite. (b) the pre-defect expands slowly. (c) by the end of 3rd charge, the pre-defect growth gives rise to new cracks in different directions shown with blue rectangles. (d) Interparticle contact loss begins to appear in the cathode composite by the end of the 4th charge. (e) The cracks and interparticle contact loss grow further by the end of the 5th charge.

All the images shown here are backscattered secondary electron images (BSE). Irrespective of the interface, crack formation and growth in LPSCl occurs either at the pre-defect or close by areas to the pre-defect. The compact area remains untouched by the growing cracks.

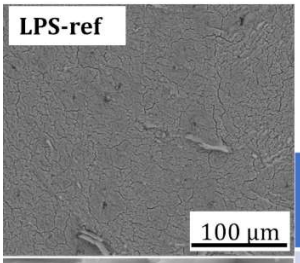

(a)

Atomic %	LPS-ref	Red cross
S	~54.9	~1.8
P	~13.9	~0.6
Ni	-	~7.2
Mn	-	~6.7
Co	-	~7.0
S/P	~3.9	~3

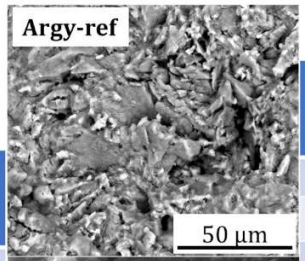

(b)

Atomic %	Argy-ref	Blue cross
S	~32.6	~4.0
P	~6.5	~1.2
Cl	~6.6	~1.2
Ni	-	~1.9
Mn	-	~2.3
Co	-	~2.0
S/P	~5.0	~3.3
S/Cl	~4.9	~3.3

ESI-8. *EDX analysis of fig 5 (a) NMC/LPS with reference -LPS (b) NMC/LPSCl with reference-LPSCl (argyrodite)*

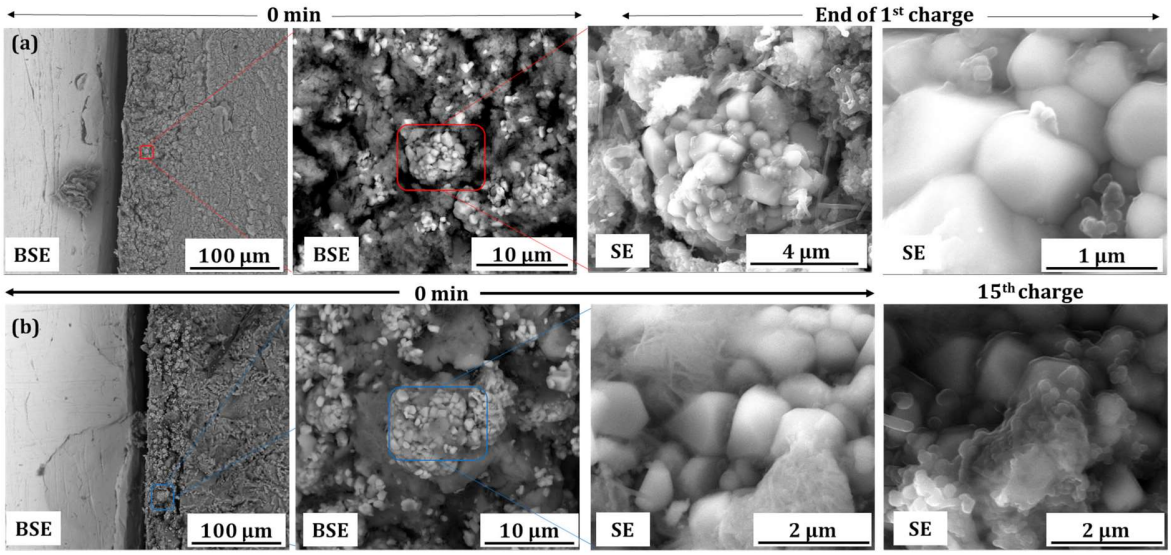

***ESI-9**. (a) Position of the secondary NMC particle in the cathode composite of LPS where surface layer/CEI is formed. This figure is used to represent the position of main figure 5 (a).*

(b) Position of the secondary NMC particle in the cathode composite of LPSCl where surface layer/CEI is formed. This figure is used to represent the position of main figure 5 (b).

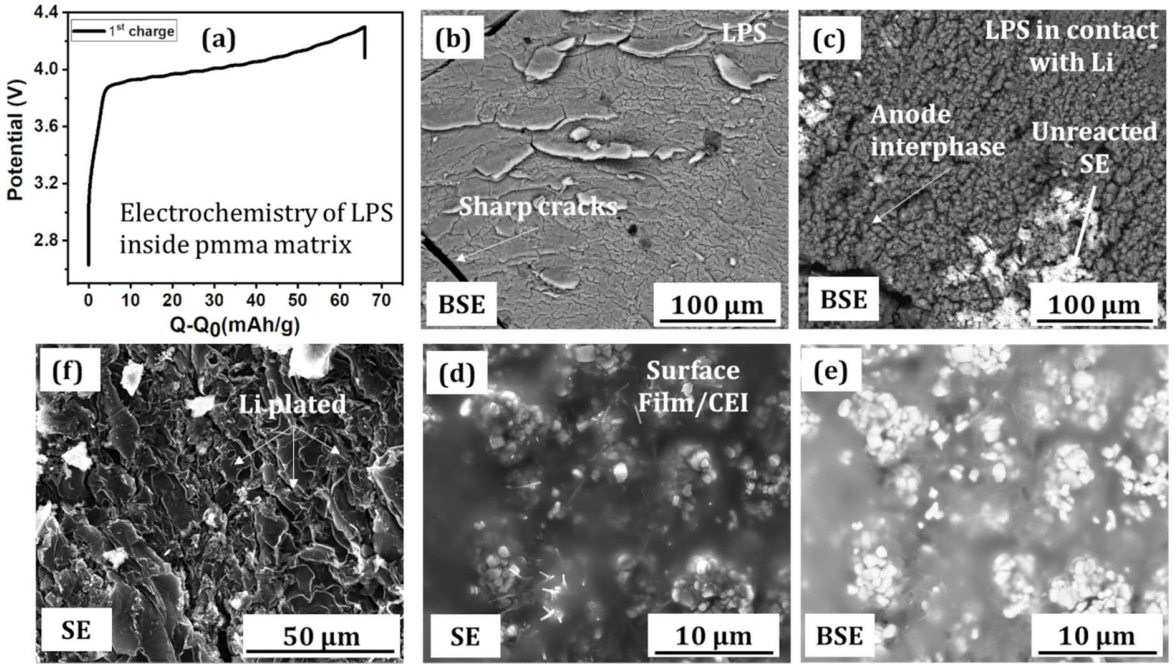

***ESI-10**. Post mortem of ex-situ cycled cell (in pmma matrix with 10 mm) with LPS-SE cycled until 1st charge only. Post mortem was carried out right after 1st charge. (a) Electrochemistry of LPS cycled at a 0.1 mA cm-2. (b) BSE image shows the observation of sharp cracks inside the LPS-SE. (c) reduced LPS-SE on the Li anode. The image contrast in the BSE image shows patches of SE that are left unreacted (d) and (e) shows the SE and BSE images showing the formation of surface layer/film on the cathode composite side facing the current collector.*

References added in the table

51 L. Zhou, K. H. Park, X. Sun, F. Lalère, T. Adermann, P. Hartmann and L. F. Nazar, *ACS Energy Letters*, 2019, **4**, 265–270.

52 H. J. Deiseroth, J. Maier, K. Weichert, V. Nickel, S. T. Kong and C. Reiner, *Journal of Inorganic and General Chemistry*, 2011, **637**, 1287–1294.

53 P. Gorai, T. Famprikis, B. S. Gill, V. Stevanovic and P. Canepa, *Chemistry of Materials*, 2020, **33**, 7484–7498.

54 S. Boulineau, M. Courty, J. Tarascon and V. Viallet, *Solid State Ionics*, 2012, **221**, 1–5.

55 and K. T. Calpa, Marcela, Hiroshi Nakajima, Shigeo Mori, Yosuke Goto, Yoshikazu Mizuguchi, Chikako Moriyoshi, Yoshihiro Kuroiwa, Nataly Carolina Rosero-Navarro, Akira Miura*, *Inorganic Chemistry*, 2021, **60**, 6964–6970.

56 M. Tachez, J. P. Malugani, R. Mercier and G. Robert, *Solid State Ionics*, 1984, **14**, 181–185.

57 Y. Seino, T. Ota, K. Takada, A. Hayashi and M. Tatsumisago, *Energy and Environmental Science*, 2014, **7**, 627–631.

58 A. Kuhn, V. Duppel and B. V. Lotsch, *Energy and Environmental Science*, 2013, **6**, 3548–3552.

59 S. A. Pervez, M. A. Cambaz, V. Thangadurai and M. Fichtner, *ACS Appl. Mater. Interfaces*, 2019, **11**, 22029.

60 B. Rolling, *J.Am.Chem.Soc*, 2013, **135**, 15694–15697.

61 A. Kuhn, O. Gerbig, C. Zhu and F. Falkenberg, *PCCP*, 2014, **16**, 14669–14674.